Vision, Modeling, and Visualization (2012)
M. Goesele, T. Grosch, B. Preim, H. Theisel, and K. Toennies (Eds.)

Visualizing Solar Dynamics Data

Gustavo M. Machado[1], Filip Sadlo[1], Thomas Müller[1], Daniel Müller[2], and Thomas Ertl[1]

[1] Visualization Research Center, University of Stuttgart, Germany
[2] European Space Agency

Abstract

Solar dynamics data, particularly those from the Solar Dynamics Observatory, are now available in a sheer volume that is hard to investigate with traditional visualization tools, which mainly display 2D images. While the challenge of data access and browsing has been solved by web-based interfaces and efforts like the Helioviewer project, the approaches so far only provide 2D visualizations. We introduce the visualization of such data in the full 3D context, providing appropriate coordinate systems and projection techniques. We also apply and extend methods from volume rendering and flow visualization to 3D magnetic fields, which we derive from the sensor data in an interactive process, and introduce space-time visualization of photospheric data. Here, we concentrate on two solar phenomena: the structure and dynamics of coronal loops, and the development of the plasma convection in close vicinity of sunspots over time. Our approach avoids the time-coherence issue inherent in traditional magnetic field line placement, providing insight in the magnetic field and the structure of the coronal plasma. We are convinced that the presented techniques are applicable in many other fields such as the terrestrial magnetospheric physics, or magnetohydrodynamics simulations.

Categories and Subject Descriptors (according to ACM CCS): Computer Graphics [I.3.8]: Applications—Physical Sciences and Engineering [J.2]: Physics—

1. Introduction

When observed at low spatial resolution in the visual part of the electromagnetic spectrum, the Sun appears as a rather unspectacular, quiescent, bright disk, and it is only during solar eclipses that details of its extended outer atmosphere, the corona, become observable from Earth. However, in the ultraviolet and X-ray regime of the spectrum, our Sun reveals its spectacular dynamic nature and the energetic processes in its atmosphere. The solar wind, which consists mainly of charged particles, continuously impinges upon the Earth's magnetic field. Single energetic events like solar flares or coronal mass ejections that are directed toward the Earth can damage power grids—as happened in Quebec/Canada in 1989—or communication satellites. A solar eruption like the one of September 1859 could cause complete power blackout. Hence, there is an increased interest in monitoring—and ultimately forecasting—the Sun's activity and the resulting space weather phenomena not only from a scientific point of view but also from a commercial one.

Currently, some of the main scientific objectives in solar research are: How does the Sun generate its magnetic field? How does that field produce flares and coronal mass ejections (CMEs)? How is the solar corona being heated? And how does the Sun influence space weather? On the way to answering these fundamental astrophysical questions, we believe that this paper and the resulting future work in solar visualization will contribute to new insights, new techniques, and eventually new models.

NASA's Solar Dynamics Observatory (SDO) is the most recent space telescope that monitors our Sun 24/7 at multiple wavelengths which results in terabytes of high-resolution raw image data every day. While browsing the huge image archive is already realized by the Helioviewer project [M*09, jhe], there is no tool for an interactive exploration of more complex data products related to physical quantities that are derived from the raw image data. This, however, is indispensable for a deeper understanding of the magnetized plasma that constitutes the solar atmosphere.

In this paper we apply visualization techniques ranging from volume visualization over flow visualization to space-time visualization, making use of the focus+context and linked views elements. We exemplify the utility of our ap-

DOI: 10.2312/PE/VMV/VMV12/095-102

proach through selected problems in solar physics in joint work with two domain experts. Their evaluations and physical backup are part of the result section.

In this paper we present the following contributions to the field of solar dynamics data visualization:

- raycasting for solar data in spherical grids,
- 3D LIC as an alternative for field line placement,
- a data-driven LIC-based technique for visualizing the magnetic field, imitating the self-illustrating phenomenon of coronal loops, and
- space-time visualization of photosphere data.

2. Related Work

Visualization looks back on a long history in astronomical research—from the conversion of sensor data to images, to the analysis of simulation results. However, while many of the involved problems are 2D and comparably well supported by appropriate visualization techniques, it is in particular the 3D structure of the Sun's magnetic field that requires visualization approaches beyond those traditionally used. This topic is gaining importance since the simulation of the 3D magnetic field of the solar corona can be driven by measurements of the magnetic field on its "surface".

Traditionally, the Sun's magnetic field is visualized by sets of field lines, suffering from the influence of the usually randomly or manually chosen seed points. Sundquist [Sun03] presents dynamic line integral convolution, Klein et al. [KE04] present an approach based on a particle model to visualize magnetic field lines, and Thomaszewski et al. [TGPS08] introduce magnetic interaction in rigid body simulations based on dipoles. Sanderson et al. [SCT*10] visualize magnetic fields in fusion reactors, Sadlo et al. [SPP04] apply magnetic visualization to vortices, and Bachthaler et al. [BSW*12] visualize 2D flux topology.

JHelioviewer by Müller et al. [M*09,jhe] is a visualization software for browsing large solar image archives using the JPEG 2000 interactive protocol. It also provides time navigation and composition of images from different wavelengths. SolarSoftWare (SSW) [ssw] is an IDL-based system which provides a common programming and data analysis environment for solar physics. In SSW, DeRosa [pfs] developed a Potential-Field Source-Surface (PFSS) viewer to show magnetic field lines based on SOHO/MDI magnetograms.

First models of the solar corona's global magnetic structure were developed by Schatten et al. [SWN69] and Altschuler and Newkirk [AN69]. They extrapolated the radial component of the magnetic field measured in the photosphere using a potential field model where electric currents are neglected and the field is forced to be radial at 1.5 solar radii above the surface. Although this is a very crude simplification, it delivers valuable results in a wide range of solar and heliospheric topics and hence it is still in use. Another extrapolation method beside PFSS is the force-free field method, see, e.g., Schrijver et al. [S*06], which implies that electric currents run only along field lines. Depending on whether the ratio of field strength to current density is constant throughout a volume or not, one refers to linear or nonlinear force-free field (NLFFF) approximation. Wiegelmann et al. [W*12] use NLFFF for the extrapolation of magnetic fields in isolated active regions and compare the resulting magnetic field lines with 171 Å SDO/AIA images. Better extrapolations for the coronal magnetic field require sophisticated magnetohydrodynamics (MHD) simulations. While these simulations can also include the solar wind and magnetic reconnection, they need massive computational resources even for small domains. A comparison of PFSS and MHD models were given by Riley et al. [R*06].

In this work, we use the PFSS model because it is easy to implement on GPUs and it delivers a good first guess of the magnetic fields in a reasonable time (order of minutes).

3. Data Sources

On a geosynchronous orbit around the Earth, the Solar Dynamics Observatory (SDO) has three main instruments onboard: the Extreme Ultraviolet Variability Experiment (EVE), the Helioseismic and Magnetic Imager (HMI), and the Atmospheric Imaging Assembly (AIA). The SDO data is available from the Joint Science Operations Center (JSOC) [jso] in the Flexible Image Transport System (FITS) image format (Pence et al. [P*10]).

It is common to give the observation time as well as the location of the observer in Carrington coordinates (CC) (θ_{CR}, ϕ_{CR}), where θ_{CR} is the Carrington latitude (CRLT) and ϕ_{CR} is the Carrington longitude (CRLN) (see Thompson [Tho06] for more details on heliographic coordinates). These coordinates "rotate with the sun" and a new Carrington rotation (CR) defines the reference meridian of the Carrington longitude.

Solar active region (AR) is the generic term for a region with an exceptionally strong magnetic activity. The Solar Region Summary (SRS) is a daily report of ARs compiled by experts from the Space Weather Prediction Center (SWPC). It contains the location of sunspot groups in heliographic coordinates as well as its area size and a classification.

The AIA instrument filters cover 10 different wavelength bands in the ultraviolet and extreme ultraviolet spectrum and map different regions of the solar atmosphere from the photosphere up to the corona. For our application, we make particular use of the 171 Å filter that is sensitive to the Fe IX line because it shows coronal loops at the best (Figure 1(a)).

The HMI instrument determines the magnetic field at the photosphere by measuring the spectral profile of the Fe I absorption line at 6173 Å (Figure 1(b)). We use HMI magnetograms, which yield the line-of-sight component of the magnetic field vector in the photosphere for various purposes,

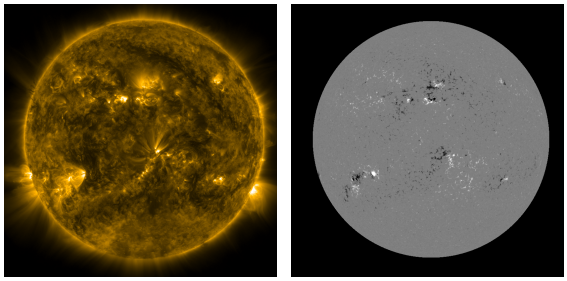

(a) (b)

Figure 1: *AIA 171 Å image (a) and HMI magnetogram (b) @ 2012.03.27, 02:02Z. (Courtesy of NASA/SDO and the AIA science team.)*

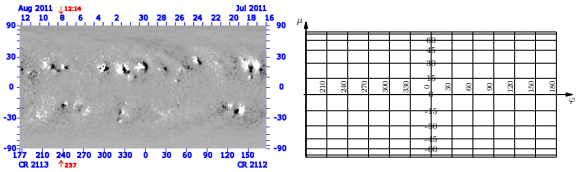

(a) (b)

Figure 2: *GONG synoptic magnetogram of 2011.08.08,12:14Z with initial Carrington longitude CRLN = 177° (a). LCEA coordinate lattice (b).*

and the HMI continuum filtergrams which provide broad-wavelength photographs of the photosphere for our 'plasma flux' texture (Section 4.5). The AIA and HMI data are resampled using supersampling on demand in regions of interest in LCEA coordinates (see below).

The Global Oscillation Network Group (GONG) [gon] is a network of six earth-bound instruments measuring the solar magnetic field and oscillations on the solar surface. The line-of-sight component of the magnetic field on the solar surface is publicly available in the form of synoptic 360° (non-synchronic) magnetograms in 360×180 pixels resolution prepared using Lambertian-Cylindrical-Equal-Area (LCEA) projection (Figure 2). This projection maps latitude θ and longitude ϕ to Cartesian coordinates (x, y) via $x = \phi - \phi_0$ and $y = \sin\theta$ with ϕ_0 being the central meridian. Synoptic magnetograms are constructed from helioprojective-Cartesian coordinates by unrolling the central meridian over time. As it delivers data for the whole solar surface, it is used to prepare a spherical harmonics (SH) decomposition. The GONG website provides the synoptic magnetograms and the SH coefficients up to order $n = 40$ with a cadence of roughly every hour. We use spherical harmonics for a global representation and the synoptic magnetograms as "space-time atlas" for overview and for selections of interesting regions.

3.1. Coronal Magnetic Field Extrapolation on GPU

While the magnetic field can readily be measured spectroscopically at the solar photosphere, this is unfortunately not feasible in the solar corona due to its much lower density. For this reason, extrapolation methods are used to reconstruct the coronal magnetic field based on photospheric data. The simplest one—the PFSS model—was developed by Altschuler and Newkirk [AN69] and Schatten et al. [SWN69]. It assumes that the coronal magnetic field is current-free, $\nabla \times \mathbf{B} = \mathbf{0}$, and thus can be represented by the gradient of a scalar potential, $\mathbf{B} = \nabla\psi$. Together with the divergence-free condition of a magnetic field, $\nabla \cdot \mathbf{B} = 0$, the scalar potential has to fulfill the Laplacian equation $\nabla^2\psi = 0$. The boundary conditions are defined on the solar surface, $R = 1$, by the magnetogram, and at the radius $r = R_w = 2.5R$ by $\psi_r = 0$, where the field is assumed to be purely radial.

The solution to the Laplacian in spherical coordinates is usually expanded into spherical harmonics (Altschuler and Newkirk [AN69]). Because direct evaluation of the spherical harmonics is computationally expensive, we resample the data on a spherical LCEA grid in a preprocessing step. Please note that we use spherical LCEA coordinates (r, μ, φ) where $\mu = \sin\theta = \cos\vartheta$ with latitude θ instead of colatitude ϑ as used in traditional spherical coordinates.

As pointed out by Tóth et al. [TvdHH11], the traditional spherical harmonics decomposition works reasonably well when the order of spherical harmonics is limited to be small relative to the resolution of the magnetogram. However, around sharp features, ringing artifacts become inevitable. Furthermore, spherical harmonics are global functions and their amplitudes depend on all of the magnetogram data. Since the basis of the spherical harmonics are the synoptic magnetograms, the global magnetic field is influenced by data that might have already changed significantly.

The finite difference method for PFSS has the advantage to be applicable also for local domains. In our application, after interactively selecting a domain on the visible side of the Sun, we define a regular curvilinear grid bounded by either $\mu = \text{const}$, $\varphi = \text{const}$, or $r = \text{const}$. The lower boundary condition, $r = R = 1$, is defined by the line-of-sight HMI magnetogram which we resample for this grid. The boundary conditions at the other five faces follow from the spherical harmonics model using the coefficients by GONG. Then, the Laplacian equation $\nabla^2\psi = 0$ yields a sparse linear system which we solve by the Krylov-type iterative method BiCGSTAB from the Cusp-library [BG12] on the GPU.

4. Visualization

The first part of our visualization stage provides the SDO data on a 3D sphere representation (Section 4.1) and focuses on the investigation of the 3D magnetic field from GONG spherical harmonics data or derived by the PFSS approach (Section 3.1), possibly obtained in an interactive manner (Section 4.6). As all are provided on spherical LCEA grids,

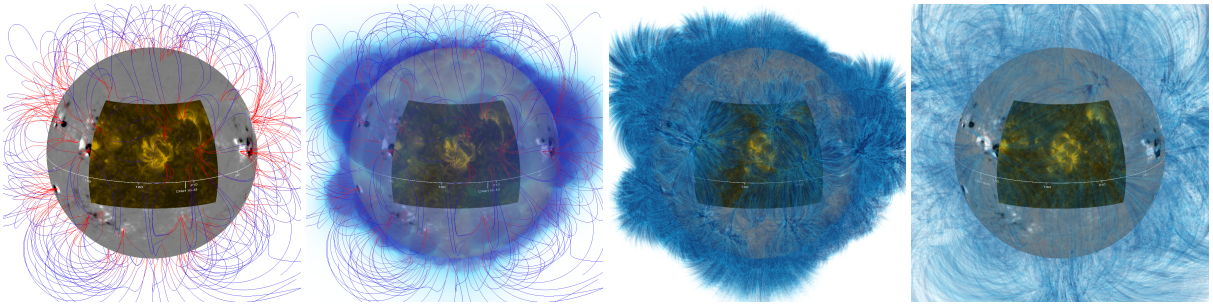

(a) (b) (c) (d)

Figure 3: *(a) Solar sphere representation with GONG synoptic data (gray) and selected region of AIA 171 Å. Visualizations of GONG SH data with field lines colored with field magnitude and additional volume rendering of magnitude (b), LIC with opacity proportional to magnitude (c), and LIC without opacity variation by field magnitude (d).*

the visualization techniques have to take this into account. To achieve interactive response times and ease implementation, we operate in *computational space* (c-space) on the GPU where applicable, including c-space field line integration (Section 4.2), c-space raycasting (Section 4.3), c-space line integral convolution (Section 4.4), and a variant thereof for visualization inspired by coronal loops (Section 4.5).

The second part (Section 4.7), realized as a linked-view, focuses on the spatiotemporal visualization of sensor data confined to the photosphere, in particular the HMI magnetograms. We apply volume rendering to reveal the space-time structure in these data and provide space-time curves of the feature classifications present as SRS data (Section 3) for context. This approach outperforms traditional temporal visualization by simple playback of the 2D SDO streams.

4.1. Solar Sphere Representation

The basis of our spatial visualization view is a spherical model of the Sun, representing the photosphere at solar radius $R = 1$. While traditional visualization tools for solar data operate in 2D plus time, we provide new possibilities and context by bringing the data from AIA, HMI, and the synoptic maps from GONG onto the solar sphere with the use of a simple raytracing approach, as illustrated in Figure 3(a). The main parametrization of our visualization are the Carrington coordinates (CC) (Section 3). We plot CRLN, CRLT, and CR on the sphere, together with an indicator showing the Earth's relative position, i.e., the current CR. As the CC system includes both a rigid body approximation of solar rotation and the motion of the Earth around the Sun, it is independent of these two mechanisms—solar features exhibit small motion in this system.

4.2. Field Line Integration

The solar sphere representation is particularly well-suited for integration with other 3D visualization techniques such as field lines (Figure 3(a)) and volume rendering. While field line integration inside uniform grids is straightforward, retrieving them from spherical grids requires some additional effort. Since we derive the field discretizations ourselves from GONG spherical harmonics or using PFSS, we have the flexibility to choose a grid type that is more appropriate for processing on GPUs. For this purpose we use structured curvilinear grids, with spherical geometry (Figure 4(a)). Hence, operations that can be performed in the *computational space* of these grids (Figure 4(b)), become straightforward and efficient on GPUs.

To solve the line integration problem in c-space, one has to adapt the magnitude and direction of the vectors with respect to the geometry of the grid. If the shape of the grid is given by a function $\Gamma(\xi)$ that maps a position ξ from c-space to p-space, the vectors would have to be transformed from p-space to c-space by multiplication with the matrix $(\nabla\Gamma(\xi))^{-1}$. This approach, however, would have two drawbacks: the difficulty of gradient estimation in curvilinear grids, and matrix inversion. We are able to avoid both problems because in case of SH or PFSS data, our vector field $\mathbf{B}$ is obtained as the gradient of the scalar potential ψ,

$$\mathbf{B} = -\nabla_x \psi = -\frac{\partial \xi}{\partial x} \nabla_\xi \psi, \tag{1}$$

where $\partial\xi/\partial x$ is the Jacobian between LCEA- and Cartesian coordinates. Hence, we simply compute the gradient only in c-space, $\beta = -\nabla_\xi \psi$, and store only β, not $\mathbf{B}$. It can be easily shown that the involved trilinear interpolation of β at ξ is identical to trilinear interpolation of $\mathbf{B}$ at $\mathbf{x}$.

4.3. Raycasting

Although, the coronal magnetic field is traditionally visualized in terms of selected field lines, their results highly depend on the selection of their seeds. By introducing volume rendering related techniques in this field, we aim at providing better tools for exploration and comparison. To avoid

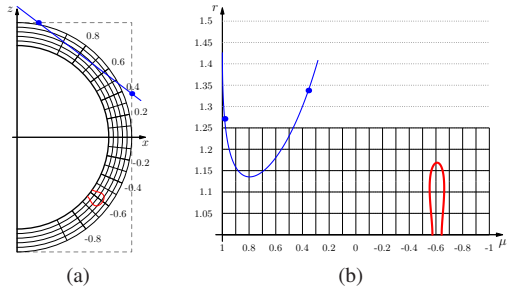

(a) (b)

Figure 4: *Spherical curvilinear grid adjacent to photosphere (bold line) in p-space (a) and in c-space (b). Raycasting (blue) in p-space would step along straight lines but along curved lines in c-space. We step along ray inside bounding box in p-space (dotted). Field line integration (red) in c-space allows for trivial and efficient point location.*

resampling, we perform raycasting also in c-space of the spherical grid. The viewing rays which are straight lines in p-space represent deformed curves in c-space (Figure 4). Although it is simple to derive a formulation of these curves in terms of c-space line integration, it would be rather costly to detect the seeds for integrating those lines, i.e., the points where the rays enter the spherical grid, in particular when only parts of the photosphere are covered by the spherical grid. Instead, we decided to stick to the p-space regarding traversal of the rays: we use standard raycasting code that marches along straight rays in p-space, limited by an axis-aligned bounding box of the possibly small spherical grid (Figure 4(a)). Only for obtaining the value of the field at the respective sample position on the ray, we transform the sample position to c-space. Figure 3(b) shows a resulting volume rendering of the field magnitude.

4.4. Line Integral Convolution

While straightforward 3D line integral convolution (LIC) often suffers from massive occlusion and visual clutter, it can provide powerful visualizations when constrained to special regions and enriched with alternative geometrical representations. In our case we do 3D LIC and typically set the opacity proportional to the field magnitude (Figure 3(c)). This readily visualizes the strong magnetic structures.

We achieve c-space LIC [For94] in 3D by simply combining the c-space line integration described in Section 4.2 with the c-space raycasting from Section 4.3. Having the magnetic field β in c-space, we simply create two additional textures (one noise and one output) in a user-defined region of interest (ROI) and at user-defined resolution. We then perform c-space integration in forward and backward directions starting at each cell of the output texture, apply the convolution with the values from the noise and store the result. The resulting texture is then raycasted in c-space. To avoid clutter and to better visualize the physical relevance of $\mathbf{B}$, we typically render the resulting texture with opacity proportional to $|\mathbf{B}|$. Note that this requires the field magnitude in p-space, not in c-space. For this, we transform β to $\mathbf{B}$ by Eq. (1).

4.5. Visualization by Virtual Coronal Loops

Particularly well seen in the spectral band around 171 Å (Figure 5(d)), the coronal loops are the building blocks of the bright X-ray and UV solar corona and subject of particularly active research. They serve as a proxy to study the time-dependent topology of the Sun's magnetic field, which is most relevant, e.g., for constraining models of solar flares and coronal mass ejections. They consist of optically thin and largely transparent plasma tracing out magnetic field lines. At the same time they undergo rapid fluctuations in intensity and shape due to plasma flows, wave phenomena, and thermodynamic fluctuations of the plasma that directly affect its emissivity. These properties make coronal loops a prominent candidate for inspection based on volume rendering techniques. However, 3D models of the global coronal plasma density are not available due to the difficulty of reconstructing the density of the optically thin, low-emission solar corona from remote-sensing observations.

We therefore present a technique to support studies of the linkage between magnetic structures observed in the Sun's photosphere and the modeled 3D magnetic field of the corona. In particular, it shall give long-term insight to which extent modern visualization techniques can be used to reproduce the appearance of coronal loops observed in AIA's 171 Å extreme ultraviolet spectral band using only data acquired in the photosphere as input. In this work, we construct a 2D texture based on a virtual plasma 'flux' at the photosphere that, combined with LIC, imitates the self-illustrating phenomenon of coronal loops.

The correlation between fine magnetic structures in the HMI magnetograms and the loops in AIA 171 Å is apparent from SDO image comparison. However, detailed inspection combined with HMI continuum data reveals that this correlation does not hold at sunspots. Thus, for the generation of a virtual 'plasma flux' texture, we clamp the magnitude of the HMI magnetogram and set it to zero using a sunspot mask built from the HMI continuum by a threshold operation.

We address the problem of plasma distribution along the magnetic field using LIC, instead of more involved and computationally more demanding advection schemes that would be able to assure mass conservation. Instead of using standard LIC with a 3D noise texture, we use our 'plasma flux' texture as 2D noise texture and locate this texture at the photosphere (see Figure 5(e)). Note that we operate in c-space, where the photosphere is planar and located at the bottom side of the grid. Specifically, we perform LIC with maximum integral curve length in both directions from each voxel, and detect if these lines intersect the 2D texture. If they do so,

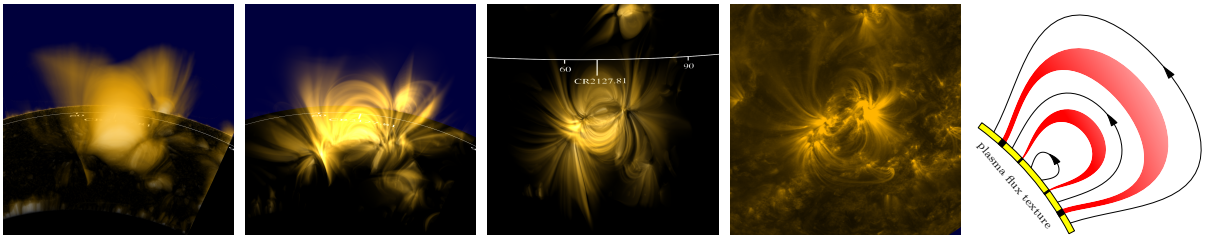

(a) (b) (c) (d) (e)

Figure 5: *(a) Visualizing coronal magnetic field (PFSS) with LIC using opacity proportional to field magnitude. (b) Same data visualized with virtual coronal loops. (c) Same as (b) but from SDO's view and (d) corresponding AIA 171 Å image. (e) The 'plasma flux' texture (yellow) is propagated along the magnetic field using LIC to produce the virtual coronal loops.*

we look up the value at the intersection points and obtain the resulting LIC value by averaging them. Otherwise the resulting LIC value is zero. This scheme distributes the values from the 2D texture in 3D along the field lines (Figure 5(e)). During rendering of the resulting LIC field, we set opacity proportional to the field magnitude, which, due to Gauss' theorem in flux tubes and the absence of divergence in magnetic fields, indirectly accounts for mass conservation. Note that it is beneficial to generate the 2D texture at higher resolution than the LIC field because this provides more detailed visualization, in particular in regions of divergent field lines. Figures 5(b) and (c) shows an example using PFSS data within a ROI, and Figure 5(a) shows, for comparison, traditional LIC with opacity proportional to field magnitude.

4.6. Interactive PFSS

Due to the absence of commonly accessible high-resolution reconstructions of the 3D coronal magnetic field, we include its extrapolation according to PFSS (Section 3.1) on the GPU. Because a full covering of the Sun would exceed typical time and storage constraints, we perform this on an interactive level, i.e., in interactively defined regions of interest. The researcher defines the upper left and lower right corner of the ROI with the mouse and these two points are transformed to LCEA coordinates on the photosphere, and the height above the solar surface is defined by numerical input. Note that typical computations take several minutes, and it is the selection of the ROI and the parametrization of the reconstruction that is interactive, although quasi-interactive reconstructions rates can be achieved from small resolutions (see Table 1). This reconstruction serves as a fast "simulation-based visualization technique" regarding the fact that more sophisticated reconstruction techniques (e.g., NLFF or MHD) are much more time consuming.

4.7. Space-Time Visualization of the Photosphere

Time-dependent solar image data are frequently displayed as time sequences or videos. Since photospheric data correspond to a narrow layer of plasma, they can be locally approximated by a 2D domain. To account for their time-dependence, they can be visualized using space-time stacking. This has, for example, been done to study so-called mesogranular flows in the photosphere using high-resolution ground-based data [R*03]. An efficient approach of this functionality by volume rendering can significantly improve the ability to quickly inspect large data sets.

We stack the data in LCEA representation, using supersampling, and visualize it within a linked view using volume rendering. Furthermore, we embed a space-time view of the SRS data as polylines to provide context. Figure 6(a) shows the selected region on the solar sphere, together with the SRS information. Figure 6(b) shows the linked view containing the space-time stack of HMI magnetograms with the time instant of the solar sphere representation indicated as a red grid plane. As the user slides through time, both views are updated accordingly. By avoiding the extraction of features, such as ridge lines or isosurfaces, our approach based on volume rendering circumvents artifacts that would typically arise due to noisy data, missing data, and fluctuations.

5. Results

As we put particular focus on the evaluation by the domain experts, they report in Section 5.1 on the results from selected cases that we already used to illustrate the techniques in Section 4. They back up their observations by astrophysics theory, evaluate the utility and possible impact of our techniques to their research area, and point out directions of future research. In Section 5.2, we conclude this part with a discussion of application-related results and measurements.

5.1. Evaluation from Domain Experts

The combination of the solar sphere representation of AIA, HMI, and GONG data, together with the field lines provides several advantages over existing techniques. The use of synoptic GONG data for full Carrington rotation overview, and the interactive replay of AIA and HMI data, together with their indicators in Carrington time substantially eases temporal and spatial navigation. Furthermore, browsing large

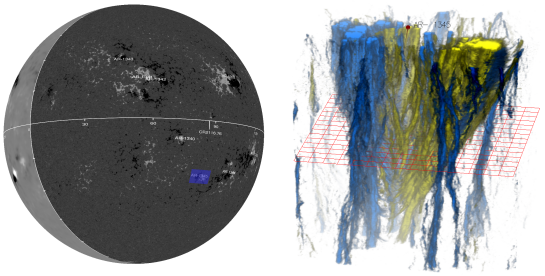

(a) (b)

Figure 6: *(a) Selection of ROI in magnetogrom data. (b) Resulting space-time HMI stack (blue: south; yellow: north), over time interval of two days in spatial region of interest, actual time indicated by red grid, with additional space-time curve of active region according to SRS data (red line).*

data sets provides an overview of large areas of the magnetic field, which makes it possible to identify regions of interest concerning specific research questions as, for example, the connectivity between several active regions.

Although, the combination of field lines with volume rendering of magnitude is an interesting alternative, achieving appropriate field line placement for representative visualization of the coronal magnetic field is an open problem. The LIC (Figure 3(d)), in contrast, is a promising alternative as it strongly reduces the risk of misinterpretation due to inappropriate field line placement. Nevertheless, LIC with opacity proportional to field magnitude (Figure 3(c)) seems to have particularly high potential in solar research because it shares the advantages of LIC but reduces clutter. Promising further work could apply LIC to more complex solar magnetic field models, which can contribute to the study of topological features like magnetic separatrices and null points that are thought to play a key role in coronal dynamics.

The technique of virtual coronal loops represents a very interesting approach for the research of coronal plasma dynamics. Observational studies of magnetograms have shown permanent changes in the photospheric magnetic field after flares. 3D visualizations of the before/after stage of such "collapsing" magnetic loop systems and especially the comparison of virtual coronal loops with observational data would provide a big step in validating the model and obtaining high number statistics. The fully interactive exploration is likely to inspire new research questions and physical models and future work shall investigate new possibilities of coronal plasma reconstruction and interactive visualization.

The integrated PFSS provides a convenient approach for extrapolating the 3D coronal field. The fact that the results can easily be visualized together with, e.g., GONG SH data allows for interactive exploration based on PFSS.

The space-time visualization technique has proven its potential as compared to traditional replay of AIA and HMI sequences. Having the space-time structure at instantaneous view, together with the active regions from SRS, provides new and exciting insight in the dynamics of the convection-dominated magnetic field, in particular in the vicinity of sunspots. Specific research questions, such as the behavior of magnetic elements that persistently stream away from sunspots, so-called moving magnetic features (MMF) require the analysis and inspection of large areas in magnetograms and their temporal evolution. The spatiotemporal visualization provides the means to identify patterns in the MMFs which are difficult to recognize in video displays.

5.2. Discussion

For the coronal magnetic field extrapolation on the GPU with PFSS we use the Cusp library [BG12] which is still in a development state and which lacks suitable preconditioners. This makes the convergence of our PFSS code rather slow. More advanced libraries (CULA) are likely to reduce the computation time. Moreover, for high resolution PFSS and LIC calculations the GPU memory consumption reaches the limits of todays graphics hardware.

For the performance measurements of our application, we used a Linux based system consisting of an Intel(R) Core(TM) i7-2600 CPU @ 3.4GHz, NVidia Geforce GTX 560 Ti graphics card with 2GB RAM, NVidia driver version 295.20, and CUDA version 4.1. Table 1 shows the performance and GPU memory consumption values for the PFSS calculation, where we have used the following region of interest: 2011-01-22, 06:00:00Z, $r/R = [1, 1.25]$, $\sin\theta = [-0.05, 0.8389]$, $\varphi = [50°, 80°]$. Table 2 shows the computation times for generating the LIC volumes. Our example of volume rendering (Figure 3(b)), with a resolution of 1200×1200 and 500 steps per ray performs with 2.48 fps. Please note that we do not use any acceleration technique.

Table 1: *Performance measurements and GPU memory consumption for PFSS calculation.*

Resolution $(\varphi, \sin\theta, r)$	GPU Mem	Computation time
$50 \times 50 \times 20$	75 MB	4.8 s
$50 \times 50 \times 60$	94 MB	26 s
$100 \times 100 \times 60$	183 MB	1 min 13 s
$150 \times 150 \times 60$	332 MB	2 min 4 s
$200 \times 200 \times 60$	539 MB	6 min 1 s
$250 \times 250 \times 60$	808 MB	9 min 22 s

Table 2: *Performance measurements for the precalculation of the LIC volume.*

Method	Resolution	time(sec)	# steps
LIC (Fig. 3(d))	$900 \times 450 \times 250$	36.18	250
LIC (Fig. 3(d))	$360 \times 180 \times 100$	2.70	250

6. Conclusion

We successfully applied visualization techniques from vector field visualization and volume rendering to solar dynamics data. While already the straightforward application of existing techniques from these fields proved valuable for solar physics research, the domain experts see high potential in their combination. In particular they expect that the space-time visualization of the magnetogram structure, and 3D LIC may become widely used tools in their field. Although they were fascinated about the virtual coronal loop visualizations, it is the technique that is hardest to interpret and validate in terms of coronal plasma dynamics. Nevertheless, since the resulting loops strictly follow the magnetic field, their utility for the visualization of the magnetic field as a method that imitates the self-illustrating phenomena of coronal loops, is out of question. They expect an enrichment in research both on the astrophysics and visualization side due to this work.

The following topics lend themselves as future work. Our space-time investigation approach is limited to phenomena on the solar surface. In the future, we want to investigate dedicated means for studying 3D phenomena, such as coronal loops or faculae and the spectral power distribution including all AIA bands, over time. The potential-field source-surface (PFSS) method is still too slow for interactive rates with reasonable resolution. Hence, we plan to incorporate suitable preconditioners as well as parallel sparse linear solvers for GPU clusters. Vector magnetograms (VM) could significantly improve the local magnetic field extrapolation using PFSS or could be used for direct visualization. Hopefully, VM will become available from the JSOC database in the near future. As PFSS is only a first guess for the magnetic field extrapolation, more sophisticated codes based on non-linear force-free field or magnetohydrodynamics methods have to be integrated. We will also test if the solar region summary, which is manually compiled by domain experts, could be complemented by automated data mining systems.

In contrast to previous visualization tools like JHelioviewer, which concentrates on 2D display, or IDL-based software packages like SSW, which has limited visualization capabilities, our application offers an integrated system for space and time navigation in a three-dimensional context, and interactive exploration of local magnetic field structure.

Acknowledgements

We thank Catherine Fisher (from ESA) for contributing to the evaluation of this work. This work was supported by Capes-Brazil (BEX 4097/10-6) and the Collaborative Research Center SFB-TRR 75 at the University of Stuttgart.

References

[AN69] ALTSCHULER M. D., NEWKIRK G.: Magnetic fields and the structure of the solar corona. *Solar Physics 9* (1969), 131–149. 2, 3

[BG12] BELL N., GARLAND M.: Cusp: Generic parallel algorithms for sparse matrix and graph computations, 2012. 3, 7

[BSW*12] BACHTHALER S., SADLO F., WEEBER R., KANTOROVICH S., HOLM C., WEISKOPF D.: Magnetic Flux Topology of 2D Point Dipoles. *Computer Graphics Forum 31*, 3 (2012), 955–964. 2

[For94] FORSSELL L. K.: Visualizing flow over curvilinear grid surfaces using line integral convolution. In *Proceedings of IEEE Visualization* (1994), pp. 240–247. 5

[gon] National Solar Observatory, Global Oscillation Network Group (GONG). http://gong.nso.edu/. 3

[jhe] JHelioviewer. http://jhelioviewer.org/. 1, 2

[jso] JSOC – Joint Science Operations Center; SDO Data access for HMI and AIA data. http://jsoc.stanford.edu/. 2

[KE04] KLEIN T., ERTL T.: Illustrating Magnetic Field Lines using a Discrete Particle Model. In *Workshop on Vision, Modelling, and Visualization (VMV)* (2004), pp. 387–394. 2

[M*09] MÜLLER D., ET AL.: JHelioviewer: Visualizing Large Sets of Solar Images Using JPEG 2000. *Computing in Science & Engineering 11*, 5 (2009), 38–47. 1, 2

[P*10] PENCE W. D., ET AL.: Definition of the Flexible Image Transport System (FITS), version 3.0. *Astronomy and Astrophysics 524* (2010), A42. 2

[pfs] Interactive Data Language (IDL) Software for Analyzing Solar Magnetic Fields. www.lmsal.com/ derosa/pfsspack. 2

[R*03] ROUDIER T., ET AL.: Families of fragmenting granules and their relation to meso- and supergranular flow fields. *Astronomy & Astrophysics 409* (2003), 299–308. 6

[R*06] RILEY P., ET AL.: A comparison between global solar magnetohydrodynamic and potential field source surface model results. *Astrophys. J. 653*, 2 (2006), 1510. 2

[S*06] SCHRIJVER C., ET AL.: Nonlinear Force-Free Modeling of Coronal Magnetic Fields Part I: A Quantitative Comparison of Methods. *Solar Physics 235* (2006), 161–190. 2

[SCT*10] SANDERSON A. R., CHEN G., TRICOCHE X., PUGMIRE D., KRUGER S., BRESLAU J.: Analysis of recurrent patterns in toroidal magnetic fields. *IEEE Transactions on Visualization and Computer Graphics 16*, 6 (2010), 1431–1440. 2

[SPP04] SADLO F., PEIKERT R., PARKINSON E.: Vorticity Based Flow Analysis and Visualization for Pelton Turbine Design Optimization. In *Proceedings of IEEE Visualization* (2004), pp. 179–186. 2

[ssw] SolarSoftWare (SSW) is an Interactive Data Language (IDL) based software library. www.lmsal.com/solarsoft. 2

[Sun03] SUNDQUIST A.: Dynamic line integral convolution for visualizing streamline evolution. *IEEE Transactions on Visualization and Computer Graphics 9*, 3 (2003), 273–282. 2

[SWN69] SCHATTEN K. H., WILCOX J. M., NESS N. F.: A model of interplanetary and coronal magnetic fields. *Solar Physics 6* (1969), 442–455. 2, 3

[TGPS08] THOMASZEWSKI B., GUMANN A., PABST S., STRASSER W.: Magnets in motion. *ACM Transactions on Graphics 27*, 5 (2008), 162:1–162:9. 2

[Tho06] THOMPSON W. T.: Coordinate systems for solar image data. *Astronomy and Astrophysics 449* (2006), 791–803. 2

[TvdHH11] TÓTH G., VAN DER HOLST B., HUANG Z.: Obtaining Potential Field Solutions with Spherical Harmonics and Finite Differences. *Astrophys. J. 732*, 2 (2011), 102. 3

[W*12] WIEGELMANN T., ET AL.: How to optimize nonlinear force-free coronal magnetic field extrapolations from SDO/HMI vector magnetograms? *arXiv:1202.3601v1* (2012). 2